Integrated Short-TE and Hadamard-edited Multi-Sequence (ISTHMUS) for Advanced MRS

Steve C.N. Hui[1,2,3†], Saipavitra Murali-Manohar[4,5†], Helge J. Zöllner[4,5], Kathleen E. Hupfeld[4,5], Christopher W. Davies-Jenkins[4,5], Aaron T. Gudmundson[4,5], Yulu Song[4,5], Vivek Yedavalli[4,5], Jessica L Wisnowski[6,7], Borjan Gagoski[8,9], Georg Oeltzschner[4,5], Richard A.E. Edden[4,5*]

[1] Developing Brain Institute, Children's National Hospital, Washington, D.C. USA
[2] Departments of Radiology, The George Washington University School of Medicine and Health Sciences, Washington, D.C. USA
[3] Departments of Pediatrics, The George Washington University School of Medicine and Health Sciences, Washington, D.C. USA
[4] The Russell H. Morgan Department of Radiology and Radiological Science, Johns Hopkins University School of Medicine, Baltimore, MD, USA
[5] F.M. Kirby Research Center for Functional Brain Imaging, Kennedy Krieger Institute, Baltimore, MD, USA
[6] Department of Radiology, Children's Hospital Los Angeles, Los Angeles, CA, USA
[7] Department of Pediatrics, Children's Hospital Los Angeles, Los Angeles, CA, USA
[8] Fetal Neonatal Neuroimaging and Developmental Science Center, Boston Children's Hospital, Boston, MA, USA
[9] Department of Radiology, Harvard Medical School, Boston, MA, USA

* Corresponding author. 600 N. Wolfe Street, Park 338, Baltimore, MD 21287, USA
Email address: raee2@jhu.edu

[†] Steve C.N. Hui and Saipavitra Murali-Manohar contributed equally to this work

Acknowledgement

This work was supported by NIH grants R01 EB016089, R01 EB023963, R21 EB033516,

R00 AG062230, K00 AG068440 and P41 EB031771.

Running title: ISTHMUS for advanced MRS

Total word count: 4422

Abstract

Purpose: To examine data quality and reproducibility using ISTHMUS, which has been implemented as the standardized MR spectroscopy sequence for the multi-site HBCD study.

Methods: The ISTHMUS acquisition included 32 transients of short-TE PRESS followed by 224 transients of long-TE HERCULES. 4 short-TE and 4 long-TE interleaved water reference scans were acquired with real-time frequency correction. Datasets were modeled using Osprey with a simulated basis set consisting of 18 metabolite functions. Measured concentrations were scaled with respect to the acquired short-TE water reference and corrected for tissue content. In vivo experiments were performed in 10 healthy volunteers (6 female; 29.5±6.6 years). Each volunteer underwent two scans on the same day. tCr linewidths were compared using one-way ANOVA. Agreement between the measurements were shown using Bland-Altman plots. Differences in metabolite measurements between the two scans were examined using paired t-test. CVs and correlations between water reference ratios and the Osprey correction factors were measured.

Results: No significant difference in linewidth was observed between PRESS and HERCULES. Bilateral thalamus produced significantly higher ($p<0.001$) linewidth compared to the other three regions. The Bland-Altman plot showed good agreement in linewidth between scan 1 and scan 2. Paired t-tests indicated a significant difference ($p=0.002$) in PRESS NAAG between the two thalamus scans. Water reference ratios and the Osprey correction factor were significantly correlated ($p<0.05$) in all four brain regions.

Conclusion: ISTHMUS enhanced the resolution of Hadamard-edited scans by the high SNR of short-TE transients and the robustness to developmental changes in transverse relaxation using the multi-TE water references.

Keywords: MR spectroscopy, PRESS, Hadamard encoding, Spectral editing, HBCD

1 INTRODUCTION

The purpose of this study was to present the Integrated Short-TE and Hadamard-edited Multi-Sequence (ISTHMUS) which consisted of a short-TE unedited PRESS (high SNR, low T_2-weighting, low resolution) (1) and a long-TE edited HERCULES (lower SNR, higher T_2-weighting, higher resolution) (2) into a single scan, delivering a range of metabolic information in a single acquisition. ISTHMUS has been implemented into the full protocol for the HEALthy Brain and Child Development (HBCD) study (3), a longitudinal study that follows children's developing brains from newborn through early childhood. The feature of this integrated sequence combines an unedited and an edited MRS sequence using PRESS localization with dual-TE water references. To make the content more legible, data acquired using the short-TE unedited PRESS will be referred to as PRESS and the long-TE edited HERCULES will be referred to as HERCULES in this manuscript. As there are pros and cons for short- and long-TE acquisitions, data acquired using both TEs in a single acquisition cover the drawback from each other. With very limited data and knowledge on metabolite T_2 relaxation times especially on neonates, a multi-TE sequence is helpful to gather more information on the T_2 decay and hence is more robust to T_2 changes. Another advantage of the ISTHMUS is lowering operator workload. In this two-in-one ISTHMUS sequence, water reference data corresponding to both PRESS and HERCULES scans are acquired. In Philips, water reference scans are collected simultaneously during the data acquisition, meaning two different acquisitions on the acquisition protocol as PRESS and HERCULES scans are combined into one. On the other hand, for Siemens users the integrated sequence will offer a substantial improvement. They are acquired as a 'separate' scan in the acquisition protocol on Siemens scanners which adds up to a total of 4 sequences (PRESS, HERCULES, short-TE water reference and long-TE water reference). ISTHMUS helps to integrate them into a single sequence which minimizes potential errors from protocol set-up and possibility of human error during data acquisition.

In vivo MRS allows for non-invasive quantification of brain metabolites but is limited by resolution due to broad in vivo linewidths (in the order of 10 Hz) and peak splitting due to J-couplings. The limited dispersion of signals along the chemical shift dimension leads to spectral overlap particularly for metabolites with low concentration. Edited MRS improves resolution through frequency-specific manipulation of known couplings in target metabolites, such as the

inhibitory neurotransmitter γ-aminobutyric acid (GABA) and the antioxidant glutathione (GSH). It has recently been accelerated by Hadamard-encoded editing including the HERMES and HERCULES experiments (2, 4-6). The HERCULES sequence measures multiple low concentration metabolites simultaneously. A major drawback of edited MRS is that longer TEs are required for optimized editing of the target metabolites. This results in T_2 decay of metabolite signals, which in turn results in reduced metabolite signal to noise ratio (SNR) and potential misinterpretation of relaxation changes as concentration changes.

In contrast, unedited MRS for high concentration metabolite measurements can be achieved using a short TE typically between 30 ms and 35 ms using PRESS localization (1). Spectra acquired at short TE are characterized by higher SNR due to lesser T_2 decay and more pronounced metabolite resonances due to lesser J-evolution. However, underlying mobile macromolecules (MM) and lipid resonances distort the metabolite spectra at short TEs (7). This artifact can be minimized by advanced post-processing with successful baseline correction and inclusion of a cohort-mean MM basis function during curve fitting (8). At short TE, Glx (glutamine + glutamate) and GABA show multiple resonance peaks between 2.05 and 2.45 ppm partially overlapped by the NAA peak making it difficult to resolve the peaks from one another and in such cases, above-mentioned editing techniques are useful to probe these metabolites.

T_2-weighting of the MRS spectrum is directly proportional to the TE. Metabolites (e.g. mI, Glx and lipid) and MM with short T_2 relaxation times are easier to detect in short-TE spectra and these signals decay with longer TE (9, 10). A short TE also allows acquisition of water references and metabolites signals with lesser T_2 weighting. This is particularly important for T_2-corrected metabolites measurements in LCM as details related to metabolites T_2 are limited, especially for young children. In current practice, age group specific relaxation times are not considered in most fitting tools when T_2 correction is performed. Metabolite measurements on a shorter TE are therefore more accurate due to a reduced dependence on assumed metabolite T_2 values.

In vivo brain metabolite T_2 relaxation times have been reported by a few studies. Most early studies reported the relaxation times of prominent singlet signals such as tNAA, tCr and tCho in 1.5T and 3.0T (10-14). A couple of other studies performed the measurements of low

concentrations metabolites with complex coupling spin systems including Asp, GABA, Glx, GSH, mI etc. (15, 16) and in different field strengths including 4.0T, 7.0T and 9.4T (17-19). Most metabolite T_2 relaxation values are reported based on adults. Comparative studies have reported inconsistent results for the change of metabolite T_2 relaxation on NAA, tCr and tCho between young and elderly individuals (20, 21). The discrepancy may result from the data collected using different field strengths and from different brain regions. Pediatric metabolite T_2 has been rarely studied as one study has covered a small group of adolescent which reports the T_2 of NAA, Cho and Cr (22). This gap in knowledge can be attributed to the nature of longer acquisition duration of experiments to measure T_2 relaxation times, which are difficult to perform in pediatric populations. ISTHMUS acquisition also offers the potential to measure T_2 relaxation times of both water and metabolites using the short- and long-TE acquisitions.

In this study, we present data and quantification of metabolite concentrations acquired using ISTHMUS, test the quality and measure the consistency of them, and describe the benefits of the sequence.

2 METHODS

ISTHMUS is integrated with short-TE PRESS (1) and long-TE HERCULES (2) acquisitions as shown in Figure 1a. PRESS is a single-shot localization sequence consisted of one slice-selective 90° excitation pulse and two slice-selective 180° refocusing pulses, applied concurrently with three orthogonal gradients (x, y and z) (1). The two refocusing pulses yield a spin echo that fully utilizes the available M_z magnetization to produce a full-intensity signal (23, 24) for an SNR-efficient acquisition. Based on PRESS localization, HERCULES is a four-step Hadamard-encoded editing scheme dedicated for simultaneous editing and multiplexed fitting of low-concentration metabolites including ascorbate (Asc), aspartate (Asp), γ-aminobutyric acid (GABA), glutathione (GSH), lactate (Lac), N-acetylaspartate (NAA), N-acetylaspartylglutamate (NAAG) and phosphorylethanolamine (PE), as well as a couple of high-concentration metabolites including Glutamine (Gln), Glutamate (Glu), Glx (Gln + Glu), myo-inositol (mI), total Creatine (tCr = Cr + PCr) and total Choline (tCho = GPC + PCh). 20-ms editing pulses are applied at: (A) 4.58 and 1.9 ppm; (B) 4.18 and 1.9 ppm; (C) 4.58 ppm; and (D) 4.18 ppm. More details are available in Oeltzschner et al (2). Based on the implementation shown in Figure 1b,

32 short-TE PRESS transients are acquired in a block at the start (TE 35 ms, FA 90 ^{o}, shown in green), followed by 224 transients of HERCULES (TE 80 ms, shown in orange). 4 transients of short-TE 35 ms water reference signal and 4 transients of long-TE 80 ms water reference signal (both shown in blue) are interleaved throughout the acquisition. Real-time frequency correction for field drift is performed based on the water frequency of the reference scans from the localized voxel, which are acquired every 32 transients (25). Additional acquisition parameters include: 3T field strength; TR 2000 ms; second-order shim, PRESS excitation/refocusing bandwidth 2200/1350 Hz; 2048 datapoints sampled at 2 kHz.

Phantom Experiments

ISTHMUS experiments were performed using a 1000 mL cylindrical phosphate-buffered saline phantom containing Cho (3mM), Cr (10mM), GABA (2mM), L-glutamic acid (10mM), L-glutamine (3mM), Lac (5mM), myo-inositol (7.5 mM), NAA (12.5 mM) and sodium azide (0.02%) at room temperature on a Philips 3T MRI scanner (Ingenia CX, Philips Healthcare, The Netherlands) using a 32-channel phased-array head coil. Scan parameters were the same as introduced in the previous section in a 3x3x3 cm^3 voxel and excitation water suppression. Duration of the scan was approximately 9 minutes.

In Vivo Experiments

ISTHMUS experiments were performed in 10 healthy volunteers (6 females and 4 males; aged 23-46; mean 29.5 ± 6.6 years) with local IRB approval in 4 brain regions using the same 3T scanner and head coil as described in the phantom experiments and CHESS water suppression. T_1-weighted MPRAGE (TR/TE/ 6.9/3.2 ms; FA 8°; 1 mm^3 isotropic resolution) was acquired for voxel positioning and tissue segmentation. Voxels were localized in the predominantly white matter centrum semiovale (CSO), the predominantly gray matter posterior cingulate cortex (PCC) both in the size of 30×26×26 mm^3, dorsal anterior cingulate cortex (dACC) 30×30×30 mm^3 and bilateral thalamus 25×36×25 mm^3 as shown in Figure 2. Participants completed two consecutive 39-minute scans, separated by a short (~10 minutes) removal from the scanner, for examining test-retest reproducibility. Exclusion criteria included contraindications for MRI and a history of neurological and psychiatric illness.

Quantification

ISTHMUS data was separated into PRESS and HERCULES data using spec2nii (26) followed by processing and linear combination modeling (LCM) using Osprey (5). The sequence-specific basis sets for PRESS and HERCULES were generated from a fully localized 2D density-matrix simulation (101×101 resolution) using real vendor pulse waveforms and sequence timings (27, 28). Simulations were accelerated by the one-dimensional projection method (29) and the use of coherence pathways filters (30). More details are available in Hui et al (27). The metabolite basis functions included ascorbate (Asc), aspartate (Asp), creatine (Cr), negative creatine methylene (-CrCH2), gamma-aminobutyric acid (GABA), glycerophosphocholine (GPC), glutamine (Gln), glutamate (Glu), glutathione (GSH), lactate (Lac), myo-inositol (mI), N-acetylaspartate (NAA), N-acetylaspartylglutamate (NAAG), phosphocholine (PCh), phosphocreatine (PCr), phosphoethanolamine (PE), scyllo-inositol (sI), and taurine (Tau). The selection of metabolites to be included was based on the neurochemical profiles observed in the healthy adult brain to avoid any quantification bias (31). Cohort-mean measured mobile macromolecule (MM) basis functions were derived as described in a previous study (32). Briefly, frequency-domain metabolite-nulled spectra were modeled using a reduced basis set (NAA, Cr, Cho, Glu) with a flexible spline of 0.1 ppm knot spacing to define the residual metabolite signals. The residual metabolite model was then subtracted from the acquired spectrum to yield a 'clean' MM spectrum (33). The simulated metabolite and measured MM basis functions were incorporated into the Osprey software for modeling. Metabolite measurements were water-scaled and tissue-corrected for tissue-specific water visibility and relaxation times based on literature values (34). Osprey-integrated SPM12 (35) was used to perform brain tissue segmentation to yield relative tissue volume fractions of gray matter (GM), white matter (WM), and cerebrospinal fluid (CSF). Visual inspection was performed to evaluate artifacts and contamination to ensure data quality according to consensus recommendations (36). Datapoints that had concentration measurement of 0 were excluded as they were interpreted as modeling failure. The water-reference spectra were modeled with a simulated water basis function in the frequency domain with a 6-parameter model (amplitude, zero-and first-order phase, Gaussian and Lorentzian line broadening, and frequency shift). For phantom data, reduced basis functions included Cr, GABA, Gln, Glu, Lac, mI, NAA, PCh and PCr were used for modeling; no lipid and MM basis functions were included.

To test the robustness from dual-TE water referencing acquired using ISTHMUS, T_2 water reference ratios were calculated,

$$R_{T2_water} = \frac{I_{TE1} \times Scaling\ factor_{TE1}}{I_{TE2} \times Scaling\ factor_{TE2}} \quad [1]$$

where I_{TE1} denotes the integral of the water reference signal at TE 35 ms and I_{TE2} denotes the integral of the water reference signal at TE 80ms. Their respective scaling factors denote the relaxation correction values to the water-scaled amplitudes.

The Osprey T_2 correction factors based upon the compositions of tissue segmentation and T_2 values of GM, WM and CSF from the literature (34, 37) at short- and long-TE (i.e. 35 ms and 80 ms) were calculated,

$$R_{T2_correct} = \frac{\sum_{i=GM,WM,CSF} f_{i,TE1} \times e^{-\frac{TE_1}{T2_i}} \times \left(1 - e^{-\frac{TR}{T1_i}}\right) \times Scaling\ factor_{TE1}}{\sum_{i=GM,WM,CSF} f_{i,TE2} \times e^{-\frac{TE_2}{T2_i}} \times \left(1 - e^{-\frac{TR}{T1_i}}\right) \times Scaling\ factor_{TE2}} \quad [2]$$

where f_i denotes the molar fraction; $T1_i$ and $T2_i$ are constant values from the literature; TE1 and TE2 denote the 35 ms short- and 80 ms long-TE. TR denotes the repetition time of 2000 ms. Their respective scaling factors for short- and long-TEs were applied for relaxation correction to the water-scaled amplitudes. The measurements of the water reference ratios at two different echo times were compared with the Osprey T_2 correction factors to validate the T_2 relaxation correction that was applied for quantification.

Statistical Analysis

All statistical analyses were performed using R v4.0.2 in RStudio v1.2.5019 (38). Data quality metrics including SNR and linewidth of the 3-ppm tCr signal were calculated for the processed metabolite spectra from PRESS and HERCULES in CSO, dACC, PCC and bilateral thalamus. SNR is defined as the ratio of the tCr singlet peak height and the detrended standard deviation of the frequency-domain spectrum between -2 and 0 ppm. Linewidth was defined as the average of the peak-measured FWHM and the FWHM of a Lorentzian model of the tCr singlet. One-way ANOVA and the Tukey's multiple comparisons were used to compare linewidths between

PRESS and HERCULES datasets. Water-scaled and tissue-corrected metabolite concentrations were measured for Asc, Asp, GABA, GSH, Lac, NAA, NAAG, tCho, tCr, Gln, Glu and mI. Coefficients of variation (CV) were calculated for each metabolite to compare the between-subject variation of metabolite measurements (i.e. CVs from the total number of measurements from 10 participants in 20 scans). Data collected from the first and second session of the scan were compared using paired t-test and visualized using a Bland-Altman plot to evaluate reproducibility of the ISTHMUS sequence. Correlations between the water reference ratios and the Osprey correction factors and their respective CVs were measured. P-values less than 0.05 were considered statistically significant. Adjusted p-values less than 0.004 (0.05/12) were considered statistically significant when repeated measurements were performed for targeted metabolites (Asc, Asp, GABA, GSH, Gln, Glu, mI, Lac, NAA, NAAG, tCho, tCr).

3 RESULTS

Phantom experiments showed successful data acquisition using ISTHMUS. The dataset was separated into PRESS and HERCULES data as shown in Figure 3. SNR and linewidth of tCr were 96.1 and 3.2 Hz for PRESS and 248.3 and 3.5 Hz for HERCULES. Metabolite concentration measurements in the phantom are shown in Table 1. NAA, PCh and tCr were comparable between the PRESS and HERCULES sum spectrum. GABA and Lac were clearly visible as shown in Figure 3c and 3d. Since the purpose of the phantom scan was to demonstrate the functionality of the ISTHMUS sequence, no quantifications and statistical analysis were performed for this part.

In vivo experiments showed successful acquisition and separation of the ISTHMUS sequence into PRESS and HERCULES data. Linewidths of tCr and the agreement of linewidth between the first and second scan are shown in Figure 4. One-way ANOVA suggested no significant differences between PRESS and HERCULES data within the same brain region as shown in Figure 4a. Similar linewidths (~5.5 Hz) were obtained in the CSO, dACC and PCC and highest linewidths were obtained in the thalamus (~7.5 Hz). Multiple comparisons suggested linewidths in the thalamus were significantly higher ($p<0.001$) than any of those in the other 3 brain regions. The Bland-Altman plot showed the agreement of linewidth between the two scans. Most of the differences fell within ±1 Hz and the maximum differences were up to approximately ±1.5 Hz as

shown in Figure 4b. SNRs were not compared since PRESS and HERCULES data were acquired using different number of transients. Linewidths from phantom and in vivo data suggested high quality data were collected.

In vivo averaged PRESS and HERCULES data of the three Hadamard combinations (green) overlaid by the multiplexed LCM (yellow) are shown in Figure 5. Multiplexed linear combination modeling (LCM) of the in vivo ISTHMUS spectra are shown in Figure 6. Conventional 'measurable' metabolites including tNAA, tCr, tCho and mI were clearly visible in the PRESS data as shown in Figure 6a. Same metabolites were observed in Figure 6b in the HERCULES sum spectrum. GABA was successfully modeled and shown in the GABA-diff spectrum (A+B-C-D) in Figure 6c. Asc, Asp, GSH, Lac , NAAG and PE were modeled in the GSH-diff spectrum (A-B+C-D) in Figure 6d. The LCM of MM and lipid were included but not shown in the figure. Quantitative metabolite concentration measurements and their CVs for the four brain regions are shown in Table 2. In HERCULES, metabolite measurements for NAA, tNAA, tCho, tCr, Gln, Glu, Glx and mI were retrieved from the sum spectrum, GABA from the first diff-spectrum (A+B-C-D) and Asc, Asp, GSH, Lac and NAAG from the second diff-spectrum (A-B+C-D). CVs from the bilateral thalamus were the highest (i.e., most variable) compared with the other three brain regions for most metabolite measurements in PRESS and HERCULES. CVs in the same brain regions between PRESS and HERCULES were relatively similar and comparable for the high concentration metabolites including mI, tNAA, tCho, tCr and Glx. The HERCULES simultaneous modeling approach yielded slightly to moderately lower CVs for Asc, Asp, GABA and Lac compared to PRESS metabolites but was worse for GSH and NAAG potentially due to overlaying of Asc and NAA respectively.

Agreement for metabolite concentration measurements between the first and second scan is shown in Figure 7. Most measurement differences between the two scans were within the 95% confidence interval (1.96 SD) showing good reproducibility of the ISTHMUS sequence. Paired t-tests revealed no significant differences in metabolite measurements between the first and the second scans in any of the four regions using the HERCULES data as shown in Supporting Figure S1; one significant difference ($p=0.002$) was observed in NAAG in the thalamus using PRESS data as shown in Supporting Figure S2. The average water reference signal ratios were calculated as 2.48, 2.32, 2.33 and 2.80 (CV: 6%, 13.1%, 8.1% and 5.6%) for CSO, dACC, PCC

and thalamus, respectively. The average Osprey correction factors were 2.20, 1.94, 1.91 and 2.26 (CV: 4.1%, 11.7%, 7.7% and 5.6%) for CSO, dACC, PCC and thalamus, respectively. These ratios were significantly correlated ($p<0.05$) in all four brain regions as shown in Figure 8.

4 DISCUSSION

ISTHMUS consisted of a short-TE unedited PRESS and a long-TE edited HERCULES along with interleaved short- and long-TE water reference scans. Data acquired from CSO, dACC, PCC and bilateral thalamus have been successfully separated into PRESS and HERCULES data and quantified.

The in vivo data were successfully modeled using Osprey. tCho, tCr, tNAA, mI and PCr were clearly visible in the PRESS and HERCULES sum spectrum; while low concentration metabolites including GABA, GSH, Asc, Asp, PE and Lac were fitted in the HERCULES GABA-diff and GSH-diff spectra. Similar fittings were observed in the phantom data except there was no GSH, Asc and Asp. Quantification of the in vivo data suggested that CVs were low for high concentration metabolites (i.e. NAA, tCho, tCr, mI) in both PRESS and HERCULES measurements. Bilateral thalamus produced the highest CVs (i.e., most variability) in most metabolites among the four brain regions in PRESS and HERCULES data. Bad shimming and potential large variations of T_2 relaxation due to accumulation of iron may contribute to the dispersion of the measurements. CVs for edited metabolites such as GABA, GSH, Asc and Lac are in line with a previous literature (2). Asc, Gln and NAAG have relatively high CVs likely due to the overlapping of Cr signal at 3.9 ppm, Glu signal at 3.7 ppm and NAA signal at 2 ppm. These overlapping metabolite signals can be ameliorated by improving the spectral resolution using a high B_0 field. Paired t-tests suggested high agreement of metabolite measurements between the first and the second scan. No significant differences are observed in HERCULES data and only NAAG measurements from the bilateral thalamus region in PRESS are significantly different between the two scans. This is likely due to the heavy overlapping of NAA and NAAG which is also hinted by the high CVs (>30) of NAAG in the bilateral thalamus region.

Small linewidths (<6 Hz in CSO, dACC and PCC and <8 Hz in thalamus) and high agreements (discrepancy < 1.5 Hz) between the first and second scan indicate good quality and consistency

of data acquisition. The bilateral thalamus yielded significantly higher linewidths (also lower SNR) than any other brain regions using PRESS and HERCULES data. Multiple factors may contribute to the higher linewidth and the lower SNR including bad shimming, nature of T_2 relaxation and the potential influence of iron accumulation. Shimming is one of the most essential factors for successful MRS scans. The inhomogeneity of the B_0 field within the volume of the defined voxel could be deteriorated by the oval geometry of the biliteral thalamus. The thalamus also has the greatest accumulation of iron besides the basal ganglia and dentate nuclei (39-41). A higher iron concentration leads to shorter T_2 and T_2* relaxation and thus broadening of the linewidth and a reduction in the SNR (42). No significant differences (all $p>0.96$) are observed in any linewidth between PRESS and HERCULES within the same brain region as shown in Figure 4a, which show good stability of data quality between the two constituent sequences in ISTHMUS. Bland-Altman plot shows good agreement in linewidths between the first and the second scan as shown in Figure 4b. Most differences fall in between the 95% confident interval (±1.96 SD). A couple of outliers have been observed in data with lower linewidths (i.e. CSO, dACC and PCC). Since the differences are small (±1.5 Hz), they are unlikely contributed by macroscopic B_0 fluctuations whether than microscopic reasons throughout the voxel e.g. the microscopic heterogeneity of the tissue within ROI (43). SNRs have not been compared between PRESS and HERCULES since they are acquired in different numbers of transient (i.e. 32 and 224 respectively).

T_2 relaxation, which occurs at different rates for metabolite and water signals, must be corrected for in vivo MRS quantification. Typically, and in community consensus methods (36), this involves using literature reference values for metabolite relaxation rates, and water rates for each major tissue compartment (GM/WM/CSF). However, such assumptions ignore documented T_2 changes with development, aging and disease, as well as finer-grain spatial heterogeneity across the brain. Errors in assumed relaxation rates propagate strongly into concentration errors especially for in vivo protocols with TE > 30 ms and TR ~ 2s. In ISTHMUS, both water and metabolite signals are acquired at two echo times, paving the way for future two-dimensional analyses that are less susceptible to T_2 errors and changes. Comparison of the predicted water reference ratios showed significant correlations with the T_2 correction factors (based on segmentation and correction values). It is interesting to note that, while correlated, there is a

meaningful bias between the measures, i.e. the 80 ms signal is smaller than predicted from reference-value T_2 relaxation applied to the 35-ms signal by about 20%. If transverse relaxation of the water signal during TE is faster than predicted from reference values, this would lead to an underestimation of metabolite levels. The extent to which reference values are appropriate will vary between studies, and it is possible that greater biases would arise in some studies of older or younger subjects, or in patient cohorts.

Single-spectrum modeling for edited spectra sacrifices valuable spectral information in return for the reliability of concentration estimations of specific metabolites. In ISTHMUS, PRESS and HERCULES spectra have been incorporated which potentially allows multi-spectrum modeling of different TEs. For multi-spectrum modeling, the sum, GABA- and GSH-difference spectra in HERCULES can be concatenated with the PRESS spectra acquired from a different TE and perform modeling simultaneously. This approach preserves information that has been lost during subtraction in conventional single-spectrum modeling. Since spectral information is intact, definition of soft constraints, especially for low-concentration metabolites, is not required resulting an improved quantification of low-concentration metabolites (44). Multi-spectrum modeling yields lower coefficients of variation and Cramér-Rao lower bounds which improves the overall concentration estimations (45, 46). By concatenating short-TE PRESS and long-TE HERCULES, fluctuations of water T_2 are less susceptible.

One of the motivations of ISTHMUS is to develop a standardized MRS sequence for the multi-site HBCD study. Centers participating in the study include research institutes and local children's hospitals using scanners from different vendors, in which operators may be less familiar with spectroscopy. The aims of the sequence are to lower the operator workload and eliminate potential human error during protocol setup for the HBCD study. In the Siemens protocol, the constitution of ISTHMUS is equivalent to 4 separate acquisitions including PRESS, HERCULES and the two water reference scans corresponding to short- and long-TE; Philips scans acquire water reference simultaneously during metabolite spectral acquisition. In ISTHMUS, they are combined into one single scan with interleaved short- and long-TE water reference scans in every 32 transients. This allows operators to run the scan in a simple manner once the protocol/exam card has been properly set up. To facilitate and standardize post-processing, ISTHMUS data can be handled by the MRS continuous automated analysis

workflow (47). This end-to-end workflow fully automates data uptake, processing, and quality review, which integrates the most up-to-date file storage and conventions for data acquired using different scanners and vendors.

Real-time frequency update is implemented into the scan with ISTHMUS. It allows frequency correction using the interleaved water reference signal which is particularly essential in a multi-modal MR acquisition protocol, such as the HBCD study, that includes fMRI and DTI sequences prior to the MRS sequence. Both fMRI and DTI sequences require rapid switching of the gradients which generates internal heat to induce frequency drift. A recent study demonstrated that a 30-minute EPI sequence could induce an average frequency drift of more than 3 Hz and the severity varies across scanners with different hardware and cooling systems (48). It is essential to have real-time correction to control the quality of the data preventing loss of signal due to spectral broadening and subtraction artifacts from the frequency shift.

Our results have been limited by using adult data collected from one single scanner of a specific vendor. Data analysis involving multiple platforms would significantly enhance the power of statistics and the conclusion drawn in this study.

5 CONCLUSION

Successful data acquisition using the newly developed ISTHMUS sequence was demonstrated. Quality metrics show consistent data between PRESS and HERCULES. Test-retest analysis shows good reproducibility and high agreement in metabolite measurements. ISTHMUS is less demanding of technologists than its constituent parts separately acquired, hopefully resulting in reduced errors and data loss. The resolution of Hadamard-edited scans is enhanced by the high SNR of short-TE transients and the robustness to developmental changes in transverse relaxation that might arise from multiplexed modeling of short- and medium-TE acquisitions.

Disclosures of Conflicts of Interest

All authors declare no conflicts of interest.

Table 1. Quantitative water-scaled metabolite concentration measurements from the phantom data.

	Cr	GABA	Gln	Glu	mI	Lac	NAA	PCh	PCr	Glx	tCr
PRESS	2.37	3.56	1.60	10.67	5.63	4.50	9.17	3.46	4.85	12.28	7.21
HERCULES sum	0.00	0.00	1.75	6.58	1.45	2.79	8.57	2.39	6.27	8.33	6.27
HERCULES diff-1	0.84	0.68	1.77	8.07	1.31	6.18	8.08	0.00	1.10	9.84	1.94
HERCULES diff-2	0.00	0.00	0.00	1.42	4.33	3.32	21.56	0.00	3.02	1.42	3.02

Table 2. Quantitative metabolite concentration measurements (SD) and coefficient of variation from the in vivo data in CSO, dACC, PCC and bilateral thalamus. The results are tissue-corrected and water-scaled. In HERCULES, measurements for tCho, tCr, Gln, Glu, Glx, mI, NAA and tNAA were acquired from the sum spectrum, GABA from the first diff (A+B-C-D) spectrum and Asc, Asp, GSH, Lac and NAAG from the second diff (A-B+C-D) spectrum.

		Asc	Asp	GABA	GSH	Gln	Glu	mI	Lac	NAA	NAAG	tNAA	Glx	tCho	tCr
	CSO	1.00	2.18	1.10	1.93	0.60	7.77	7.21	0.59	15.19	2.80	17.99	8.18	2.54	9.61
		(0.49)	(0.35)	(0.45)	(0.34)	(0.46)	(0.91)	(0.78)	(0.4)	(1.05)	(0.49)	(0.84)	(0.94)	(0.22)	(0.53)
	CV	49	16	41	17	76	12	11	67	7	18	5	11	9	6
	dACC	1.36	2.89	1.79	2.77	2.15	12.19	9.89	0.74	16.59	1.60	18.19	14.34	2.75	11.62
		(0.83)	(0.70)	(0.68)	(0.42)	(0.94)	(1.33)	(0.91)	(0.53)	(0.93)	(0.51)	(1.02)	(1.77)	(0.18)	(0.74)
	CV	61	24	38	15	44	11	9	71	6	32	6	12	7	6
	PCC	1.33	2.83	1.60	2.23	3.98	12.42	9.72	0.30	16.30	2.06	18.36	16.40	2.06	12.14
		(0.63)	(0.36)	(0.56)	(0.38)	(0.84)	(0.91)	(1.27)	(0.18)	(1.58)	(0.55)	(1.19)	(0.98)	(0.23)	(0.84)
	CV	48	13	35	17	21	7	13	59	10	27	6	6	11	7
		1.31	1.45	0.78	2.22	1.30	7.26	8.76	0.86	15.30	1.73	17.04	8.50	3.21	11.83
	Thal	(1.08)	(0.66)	(0.79)	(0.41)	(0.77)	(1.66)	(1.81)	(0.7)	(2.3)	(0.58)	(2.5)	(2.12)	(0.52)	(1.98)
	CV	83	46	102	19	59	23	21	81	15	33	15	25	16	17
HERCULES	CSO	0.93	4.07	0.99	1.76	1.19	6.47	8.76	0.53	16.90	3.44	20.33	7.66	2.72	9.08
		(0.45)	(0.62)	(0.35)	(0.36)	(0.46)	(0.72)	(0.79)	(0.17)	(0.92)	(1.2)	(0.9)	(0.93)	(0.22)	(0.46)
	CV	49	15	36	21	39	11	9	32	5	35	4	12	8	5
	dACC	1.33	4.39	1.78	2.91	1.40	9.73	11.71	0.82	17.85	0.77	19.53	11.12	3.02	11.00
		(0.59)	(1.12)	(0.38)	(0.66)	(0.56)	(1.07)	(1.02)	(0.21)	(0.94)	(0.35)	(1.05)	(1.47)	(0.24)	(0.7)
	CV	44	26	22	23	40	11	9	26	5	46	5	13	8	6
	PCC	1.73	6.22	2.15	2.63	1.81	9.95	12.63	0.74	17.83	0.84	20.24	11.76	2.31	11.67
		(0.46)	(0.65)	(0.38)	(0.65)	(0.66)	(1.21)	(1.18)	(0.58)	(0.82)	(0.51)	(0.72)	(1.55)	(0.19)	(0.53)
	CV	27	10	18	25	36	12	9	78	5	60	4	13	8	5
	Thal	1.31	4.50	2.24	2.85	0.54	6.03	10.33	0.81	16.83	3.68	19.11	6.49	3.37	10.60
		(1.18)	(1.15)	(0.66)	(0.98)	(0.39)	(1.19)	(1.75)	(0.43)	(2.49)	(1.18)	(2.91)	(1.3)	(0.59)	(1.67)
	CV	90	26	29	34	73	20	17	53	15	32	15	20	17	16

Figure legend

Figure 1a. ISTHMUS combines a 35 ms short-TE unedited scheme (green) and a 80 ms long-TE edited HERCULES scheme (orange) using PRESS localization. Four 20-ms editing pulses (black) targeting 1.9 ppm, 4.18 ppm and 4.56 ppm are applied for Hadamard combinations. 1b. ISTHMUS multi-sequence schedule starting with 32 transients of short-TE acquisition (green) followed by 224 transients of long-TE edited HERCULES scheme (orange). 4 long- and 4 short-TE interleaved water reference scans (blue) are acquired evenly throughout the sequence.

Figure 2. Voxel locations of CSO (30×26×26 mm^3), dACC (30×30×30 mm^3), PCC (30×26×26 mm^3) and bilateral thalamus (25×36×25 mm^3).

Figure 3. Modeling of the phantom data. 3a) Short-TE unedited PRESS and 3b) long-TE HERCULES sum clearly show conventional unedited metabolites. 3c) Hadamard combinations spectra for modeling GABA, and 3d) Hadamard combinations spectra for modeling Lac. The phosphate-buffered saline phantom contains Cho, Cr, GABA, Glu, Gln, Lac, mI and NAA. Asc, Asp, GSH and NAAG were not included.

Figure 4a). Box plots depicting linewidths of tCr in four brain regions. Multiple comparisons suggested no significant difference between PRESS and HERCULES within the same brain region and linewidths in the thalamus are significantly higher compared to those in the other regions. 4b) shows the Bland–Altman plot for the agreement of linewidth between the first and the second scan.

Figure 5. Modeling of the in vivo data from CSO, 5a) showing the short-TE unedited spectrum and the three Hadamard combinations of 5b) sum, 5c) GABA-diff and 5d) GSH-diff. Unedited and edited metabolites are clearly visible.

Figure 6. Multiplexed linear modeling of the in vivo short-TE unedited and long-TE edited HERCULES spectra from CSO. Five unedited metabolites (Gln, Glu, mI, tCr, tCho) can be measured in the short-TE (6a) and long-TE sum spectrum (6b) and seven edited metabolites (Asc, Asp, GABA, GSH, Lac, NAA, NAAG) can be measured in the edited spectrum (6c and 6d).

Figure 7. Bland-Altman plot of difference against mean metabolite measurements between the first and the second scan for 7a) PRESS and 7b) HERCULES. Since the plot includes metabolite measurements from all twelve metabolites in four brain regions, the SD lines are not included because they are not representative to all data.

Figure 8. Scatter plot for T_2 water reference ratios and Osprey correction factors. They are significantly correlated ($p<0.05$) for all four brain regions. This suggests a potential benefit of the ISTHMUS dual-TE acquisition where the multi-TE water references data acquired can be used to correct T_2 relaxation for data from pediatric cohorts.

References

1. Bottomley PA. Spatial localization in NMR spectroscopy in vivo. Ann N Y Acad Sci. 1987;508:333-48.
2. Oeltzschner G, Saleh MG, Rimbault D, Mikkelsen M, Chan KL, Puts NAJ, et al. Advanced Hadamard-encoded editing of seven low-concentration brain metabolites: Principles of HERCULES. Neuroimage. 2019;185:181-90.
3. Jordan CJ, Weiss SRB, Howlett KD, Freund MP. Introduction to the Special Issue on "Informing Longitudinal Studies on the Effects of Maternal Stress and Substance Use on Child Development: Planning for the HEALthy Brain and Child Development (HBCD) Study". Advers Resil Sci. 2020;1(4):217-21.
4. Chan KL, Puts NA, Schar M, Barker PB, Edden RA. HERMES: Hadamard encoding and reconstruction of MEGA-edited spectroscopy. Magn Reson Med. 2016;76(1):11-9.
5. Saleh MG, Oeltzschner G, Chan KL, Puts NAJ, Mikkelsen M, Schar M, et al. Simultaneous edited MRS of GABA and glutathione. Neuroimage. 2016;142:576-82.
6. Chan KL, Saleh MG, Oeltzschner G, Barker PB, Edden RAE. Simultaneous measurement of Aspartate, NAA, and NAAG using HERMES spectral editing at 3 Tesla. Neuroimage. 2017;155:587-93.
7. Cudalbu C, Mlynarik V, Gruetter R. Handling macromolecule signals in the quantification of the neurochemical profile. J Alzheimers Dis. 2012;31 Suppl 3:S101-15.
8. Zollner HJ, Davies-Jenkins CW, Murali-Manohar S, Gong T, Hui SCN, Song Y, et al. Feasibility and implications of using subject-specific macromolecular spectra to model short echo time magnetic resonance spectroscopy data. NMR Biomed. 2023;36(3):e4854.
9. Cudalbu C, Behar KL, Bhattacharyya PK, Bogner W, Borbath T, de Graaf RA, et al. Contribution of macromolecules to brain (1) H MR spectra: Experts' consensus recommendations. NMR Biomed. 2021;34(5):e4393.
10. Mlynarik V, Gruber S, Moser E. Proton T (1) and T (2) relaxation times of human brain metabolites at 3 Tesla. NMR Biomed. 2001;14(5):325-31.
11. Traber F, Block W, Lamerichs R, Gieseke J, Schild HH. 1H metabolite relaxation times at 3.0 tesla: Measurements of T1 and T2 values in normal brain and determination of regional differences in transverse relaxation. J Magn Reson Imaging. 2004;19(5):537-45.
12. Barker PB, Hearshen DO, Boska MD. Single-voxel proton MRS of the human brain at 1.5T and 3.0T. Magn Reson Med. 2001;45(5):765-9.
13. Zaaraoui W, Fleysher L, Fleysher R, Liu S, Soher BJ, Gonen O. Human brain-structure resolved T(2) relaxation times of proton metabolites at 3 Tesla. Magn Reson Med. 2007;57(6):983-9.
14. Brief EE, Whittall KP, Li DK, MacKay AL. Proton T2 relaxation of cerebral metabolites of normal human brain over large TE range. NMR Biomed. 2005;18(1):14-8.
15. Ganji SK, Banerjee A, Patel AM, Zhao YD, Dimitrov IE, Browning JD, et al. T2 measurement of J-coupled metabolites in the human brain at 3T. NMR Biomed. 2012;25(4):523-9.
16. Wyss PO, Bianchini C, Scheidegger M, Giapitzakis IA, Hock A, Fuchs A, et al. In vivo estimation of transverse relaxation time constant (T(2)) of 17 human brain metabolites at 3T. Magn Reson Med. 2018;80(2):452-61.

17. Michaeli S, Garwood M, Zhu XH, DelaBarre L, Andersen P, Adriany G, et al. Proton T2 relaxation study of water, N-acetylaspartate, and creatine in human brain using Hahn and Carr-Purcell spin echoes at 4T and 7T. Magn Reson Med. 2002;47(4):629-33.
18. Marjanska M, Auerbach EJ, Valabregue R, Van de Moortele PF, Adriany G, Garwood M. Localized 1H NMR spectroscopy in different regions of human brain in vivo at 7 T: T2 relaxation times and concentrations of cerebral metabolites. NMR Biomed. 2012;25(2):332-9.
19. Murali-Manohar S, Borbath T, Wright AM, Soher B, Mekle R, Henning A. T(2) relaxation times of macromolecules and metabolites in the human brain at 9.4 T. Magn Reson Med. 2020;84(2):542-58.
20. Brooks JC, Roberts N, Kemp GJ, Gosney MA, Lye M, Whitehouse GH. A proton magnetic resonance spectroscopy study of age-related changes in frontal lobe metabolite concentrations. Cereb Cortex. 2001;11(7):598-605.
21. Marjanska M, Emir UE, Deelchand DK, Terpstra M. Faster metabolite (1)H transverse relaxation in the elder human brain. PLoS One. 2013;8(10):e77572.
22. Kirov, II, Fleysher L, Fleysher R, Patil V, Liu S, Gonen O. Age dependence of regional proton metabolites T2 relaxation times in the human brain at 3 T. Magn Reson Med. 2008;60(4):790-5.
23. Zhong K, Ernst T. Localized in vivo human 1H MRS at very short echo times. Magn Reson Med. 2004;52(4):898-901.
24. Hamilton G, Middleton MS, Bydder M, Yokoo T, Schwimmer JB, Kono Y, et al. Effect of PRESS and STEAM sequences on magnetic resonance spectroscopic liver fat quantification. J Magn Reson Imaging. 2009;30(1):145-52.
25. Edden RA, Oeltzschner G, Harris AD, Puts NA, Chan KL, Boer VO, et al. Prospective frequency correction for macromolecule-suppressed GABA editing at 3T. J Magn Reson Imaging. 2016;44(6):1474-82.
26. Clarke WT, Bell TK, Emir UE, Mikkelsen M, Oeltzschner G, Shamaei A, et al. NIfTI-MRS: A standard data format for magnetic resonance spectroscopy. Magn Reson Med. 2022;88(6):2358-70.
27. Hui SCN, Saleh MG, Zollner HJ, Oeltzschner G, Fan H, Li Y, et al. MRSCloud: A cloud-based MRS tool for basis set simulation. Magn Reson Med. 2022;88(5):1994-2004.
28. Simpson R, Devenyi GA, Jezzard P, Hennessy TJ, Near J. Advanced processing and simulation of MRS data using the FID appliance (FID-A)-An open source, MATLAB-based toolkit. Magn Reson Med. 2017;77(1):23-33.
29. Zhang Y, An L, Shen J. Fast computation of full density matrix of multispin systems for spatially localized in vivo magnetic resonance spectroscopy. Med Phys. 2017;44(8):4169-78.
30. Bodenhausen G, Kogler H, Ernst RR. Selection of coherence-transfer pathways in NMR pulse experiments. 1984. J Magn Reson. 2011;213(2):276-94.
31. Tkac I, Oz G, Adriany G, Ugurbil K, Gruetter R. In vivo 1H NMR spectroscopy of the human brain at high magnetic fields: metabolite quantification at 4T vs. 7T. Magn Reson Med. 2009;62(4):868-79.
32. Hui SCN, Gong T, Zollner HJ, Song Y, Murali-Manohar S, Oeltzschner G, et al. The macromolecular MR spectrum does not change with healthy aging. Magn Reson Med. 2022;87(4):1711-9.
33. Zollner HJ, Davies-Jenkins CW, Murali-Manohar S, Gong T, Hui SCN, Song Y, et al. Feasibility and implications of using subject-specific macromolecular spectra to model short echo time magnetic resonance spectroscopy data. NMR Biomed. 2022:e4854.

34. Wansapura JP, Holland SK, Dunn RS, Ball WS, Jr. NMR relaxation times in the human brain at 3.0 tesla. J Magn Reson Imaging. 1999;9(4):531-8.
35. Friston KJ, Holmes AP, Worsley KJ, Poline JP, Frith CD, Frackowiak RSJ. Statistical parametric maps in functional imaging: A general linear approach. Human Brain Mapping. 1994;2(4):189-210.
36. Wilson M, Andronesi O, Barker PB, Bartha R, Bizzi A, Bolan PJ, et al. Methodological consensus on clinical proton MRS of the brain: Review and recommendations. Magn Reson Med. 2019;82(2):527-50.
37. Piechnik SK, Evans J, Bary LH, Wise RG, Jezzard P. Functional changes in CSF volume estimated using measurement of water T2 relaxation. Magn Reson Med. 2009;61(3):579-86.
38. RStudioTeam. RStudio: Integrated Development for R. RStudio, PBC. Boston, MA2020.
39. Ward RJ, Zucca FA, Duyn JH, Crichton RR, Zecca L. The role of iron in brain ageing and neurodegenerative disorders. Lancet Neurol. 2014;13(10):1045-60.
40. McNeill A, Gorman G, Khan A, Horvath R, Blamire AM, Chinnery PF. Progressive brain iron accumulation in neuroferritinopathy measured by the thalamic T2* relaxation rate. AJNR Am J Neuroradiol. 2012;33(9):1810-3.
41. Peran P, Cherubini A, Luccichenti G, Hagberg G, Demonet JF, Rascol O, et al. Volume and iron content in basal ganglia and thalamus. Hum Brain Mapp. 2009;30(8):2667-75.
42. Wood JC, Enriquez C, Ghugre N, Tyzka JM, Carson S, Nelson MD, et al. MRI R2 and R2* mapping accurately estimates hepatic iron concentration in transfusion-dependent thalassemia and sickle cell disease patients. Blood. 2005;106(4):1460-5.
43. Juchem C, de Graaf RA. B(0) magnetic field homogeneity and shimming for in vivo magnetic resonance spectroscopy. Anal Biochem. 2017;529:17-29.
44. Oeltzschner G, Zupan G, Edden R, editors. Simultaneous linear-combination modeling of MEGA-PRESS sum and difference spectra without soft constraints. Proc Intl Soc Mag Reson Med 27; 0510; 2019; Montreal.
45. Rimbault DL, Oeltzschner G, Alhamud A, Meintjes E, Edden RAE, editors. Simultaneous modeling of sum and difference spectra improves quantitative outcomes for edited MRS. Proc Intl Soc Mag Reson Med 26; 1316; 2018; Paris.
46. Rotaru D, Oeltzschner G, Edden R, Lythgoe D, editors. HERCULES and ConCAT: Simultaneous modelling and fitting of 11 metabolites using LCModel. Proc Intl Soc Mag Reson Med 28; 0368; 2020.
47. Zollner HJ, Davies-Jenkins CW, Lee EG, Hendrickson TJ, Clarke WT, Edden RAE, et al. Continuous Automated Analysis Workflow for MRS Studies. J Med Syst. 2023;47(1):69.
48. Hui SCN, Mikkelsen M, Zollner HJ, Ahluwalia V, Alcauter S, Baltusis L, et al. Frequency drift in MR spectroscopy at 3T. Neuroimage. 2021;241:118430.

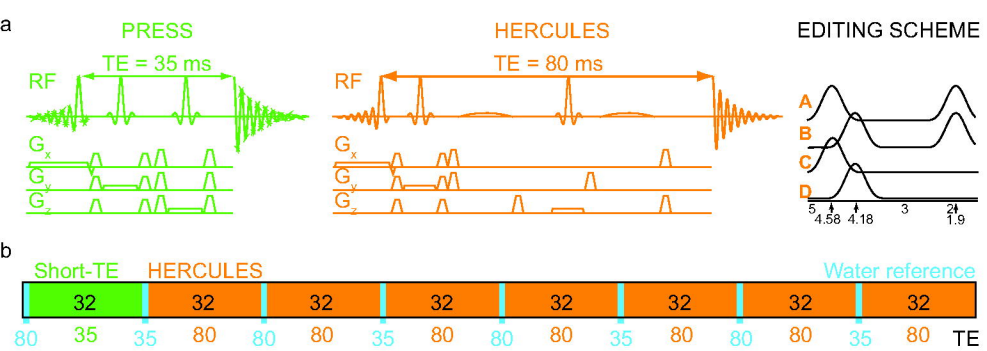
a
PRESS
TE = 35 ms
RF
Gx
Gy
Gz
HERCULES
TE = 80 ms
RF
Gx
Gy
Gz
EDITING SCHEME
A
B
C
D
5
4.58
4.18
3
2
1.9
b
Short-TE
HERCULES
Water reference
32
32
32
32
32
32
32
32
80
35
35
80
80
80
35
80
80
80
35
80
80
80
35
80
TE

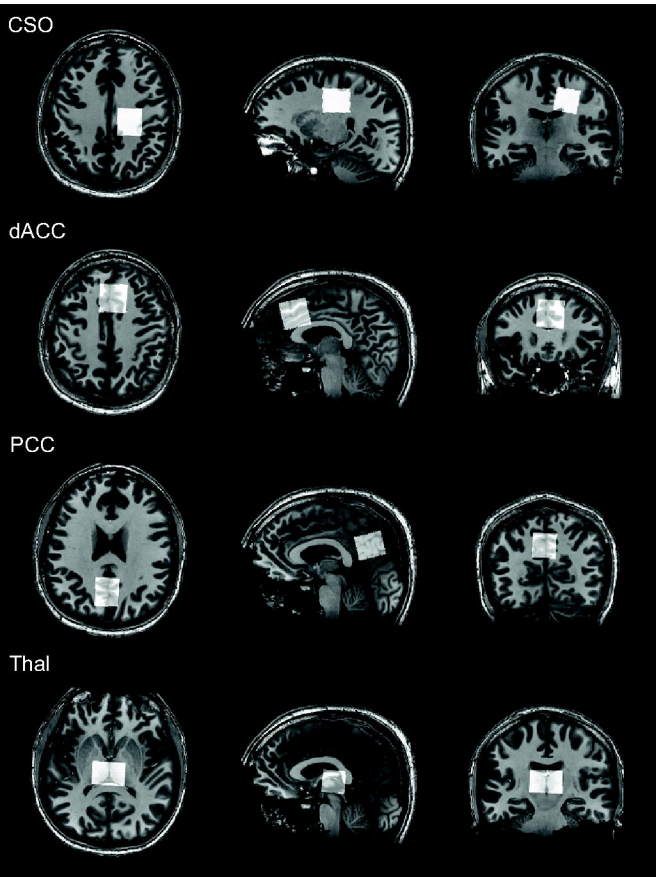
CSO
dACC
PCC
Thal

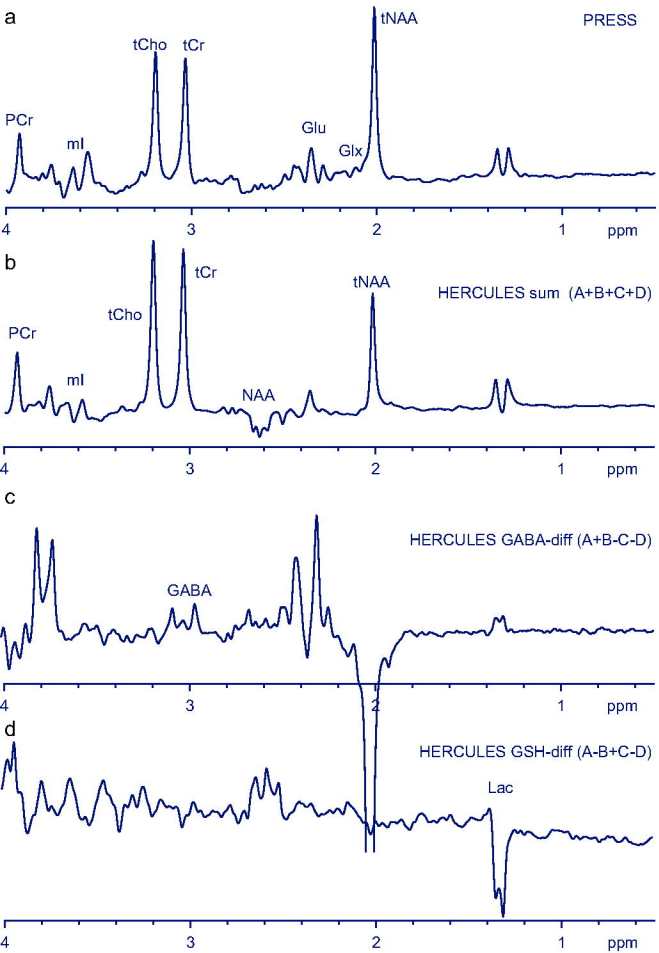
a
PRESS
tNAA
tCho
tCr
PCr
mI
Glu
Glx
4
3
2
1
ppm
b
HERCULES sum (A+B+C+D)
tCr
tNAA
tCho
PCr
mI
NAA
4
3
2
1
ppm
c
HERCULES GABA-diff (A+B-C-D)
GABA
4
3
2
1
ppm
d
HERCULES GSH-diff (A-B+C-D)
Lac
4
3
2
1
ppm

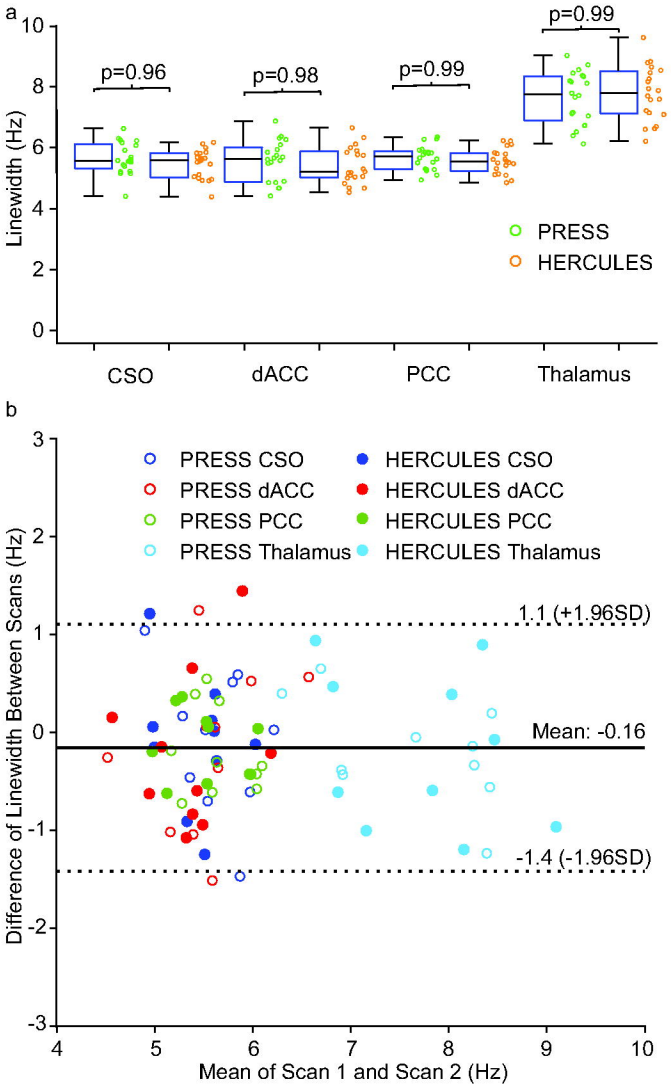
a
Linewidth (Hz)
p=0.96
p=0.98
p=0.99
p=0.99
PRESS
HERCULES
CSO
dACC
PCC
Thalamus
b
PRESS CSO
PRESS dACC
PRESS PCC
PRESS Thalamus
HERCULES CSO
HERCULES dACC
HERCULES PCC
HERCULES Thalamus
1.1 (+1.96SD)
Mean: -0.16
-1.4 (-1.96SD)
Difference of Linewidth Between Scans (Hz)
Mean of Scan 1 and Scan 2 (Hz)

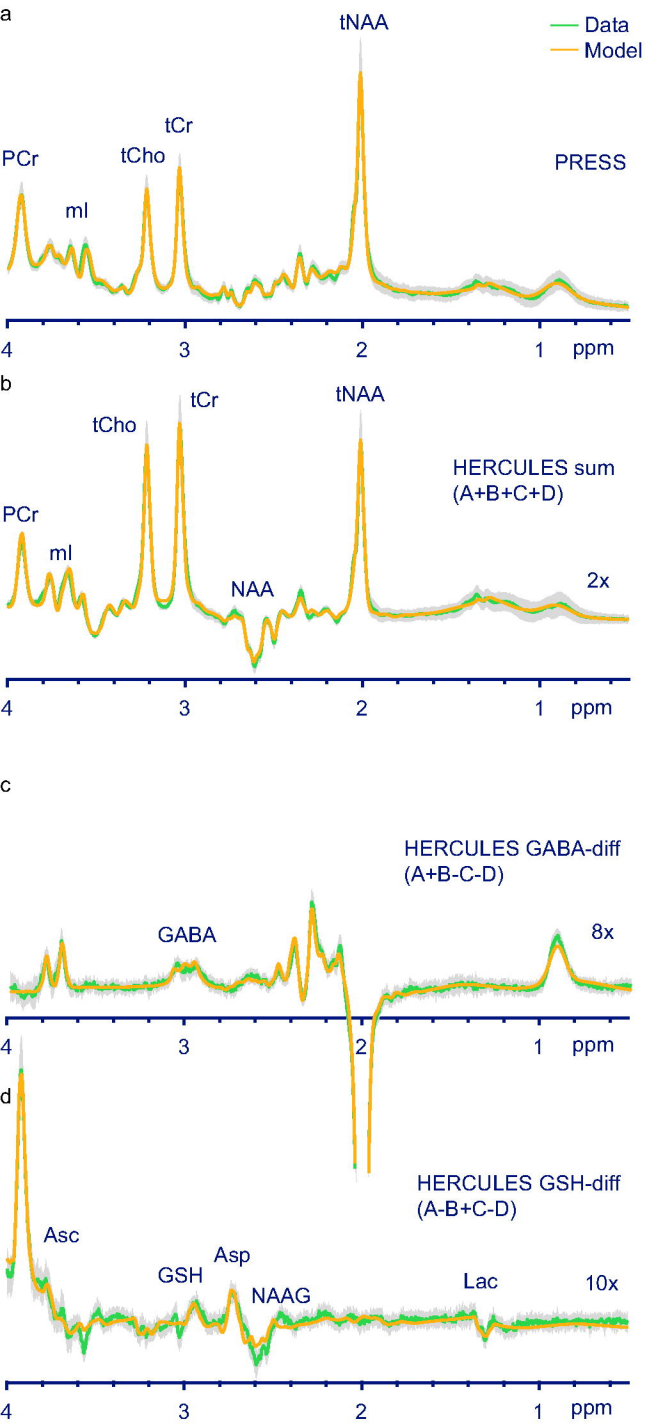
a
tNAA
Data
Model
tCr
PCr
tCho
PRESS
mI
4
3
2
1
ppm
b
tCho
tCr
tNAA
HERCULES sum
(A+B+C+D)
PCr
mI
NAA
2x
4
3
2
1
ppm
c
HERCULES GABA-diff
(A+B-C-D)
GABA
8x
4
3
2
1
ppm
d
HERCULES GSH-diff
(A-B+C-D)
Asc
Asp
GSH
NAAG
Lac
10x
4
3
2
1
ppm

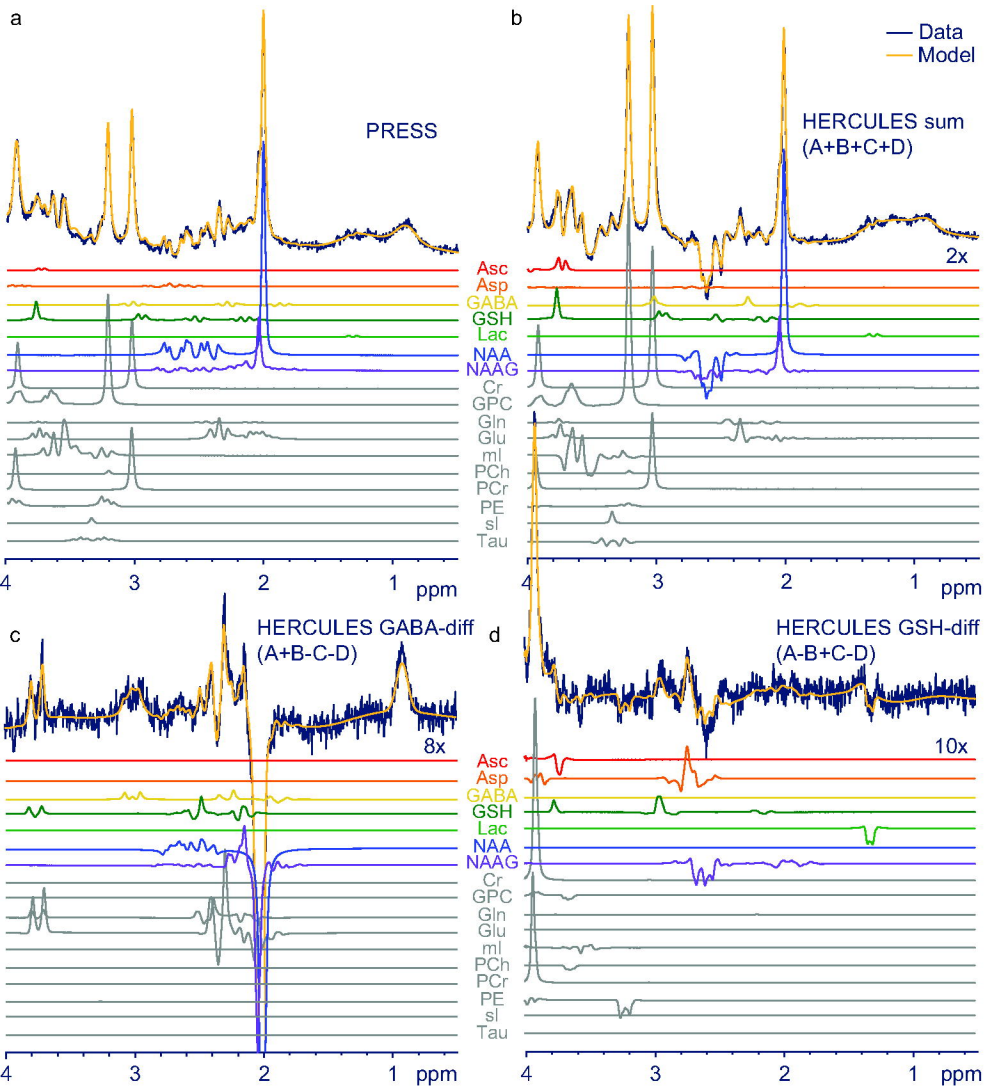
a
PRESS
b
Data
Model
HERCULES sum
(A+B+C+D)
2x
Asc
Asp
GABA
GSH
Lac
NAA
NAAG
Cr
GPC
Gln
Glu
mI
PCh
PCr
PE
sI
Tau
4
3
2
1
ppm
c
HERCULES GABA-diff
(A+B-C-D)
8x
d
HERCULES GSH-diff
(A-B+C-D)
10x

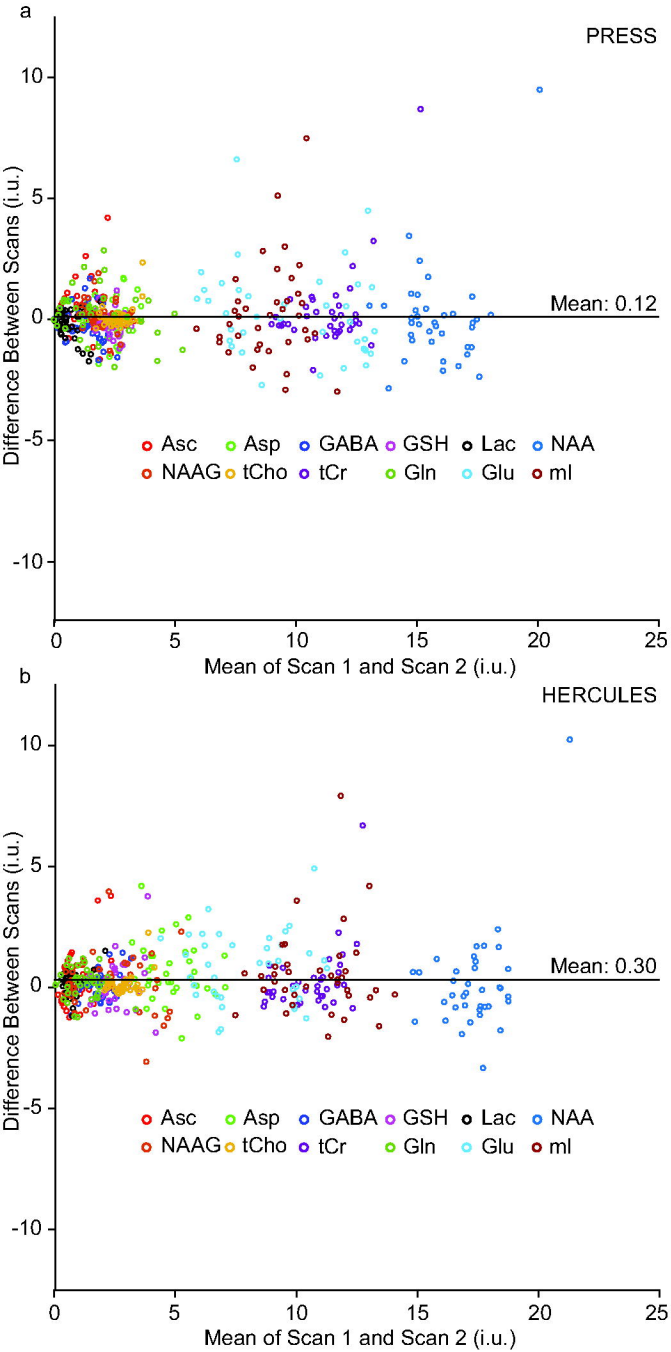
a
PRESS
Mean: 0.12
Difference Between Scans (i.u.)
Mean of Scan 1 and Scan 2 (i.u.)
Asc
Asp
GABA
GSH
Lac
NAA
NAAG
tCho
tCr
Gln
Glu
ml
b
HERCULES
Mean: 0.30
Difference Between Scans (i.u.)
Mean of Scan 1 and Scan 2 (i.u.)
Asc
Asp
GABA
GSH
Lac
NAA
NAAG
tCho
tCr
Gln
Glu
ml

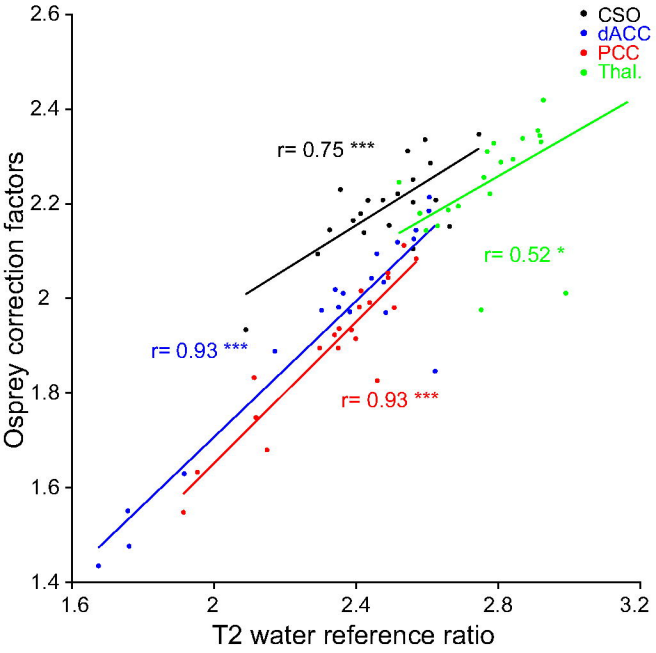
CSO
dACC
PCC
Thal.
r= 0.75 ***
r= 0.52 *
r= 0.93 ***
r= 0.93 ***
Osprey correction factors
T2 water reference ratio
2.6
2.4
2.2
2
1.8
1.6
1.4
1.6
2
2.4
2.8
3.2

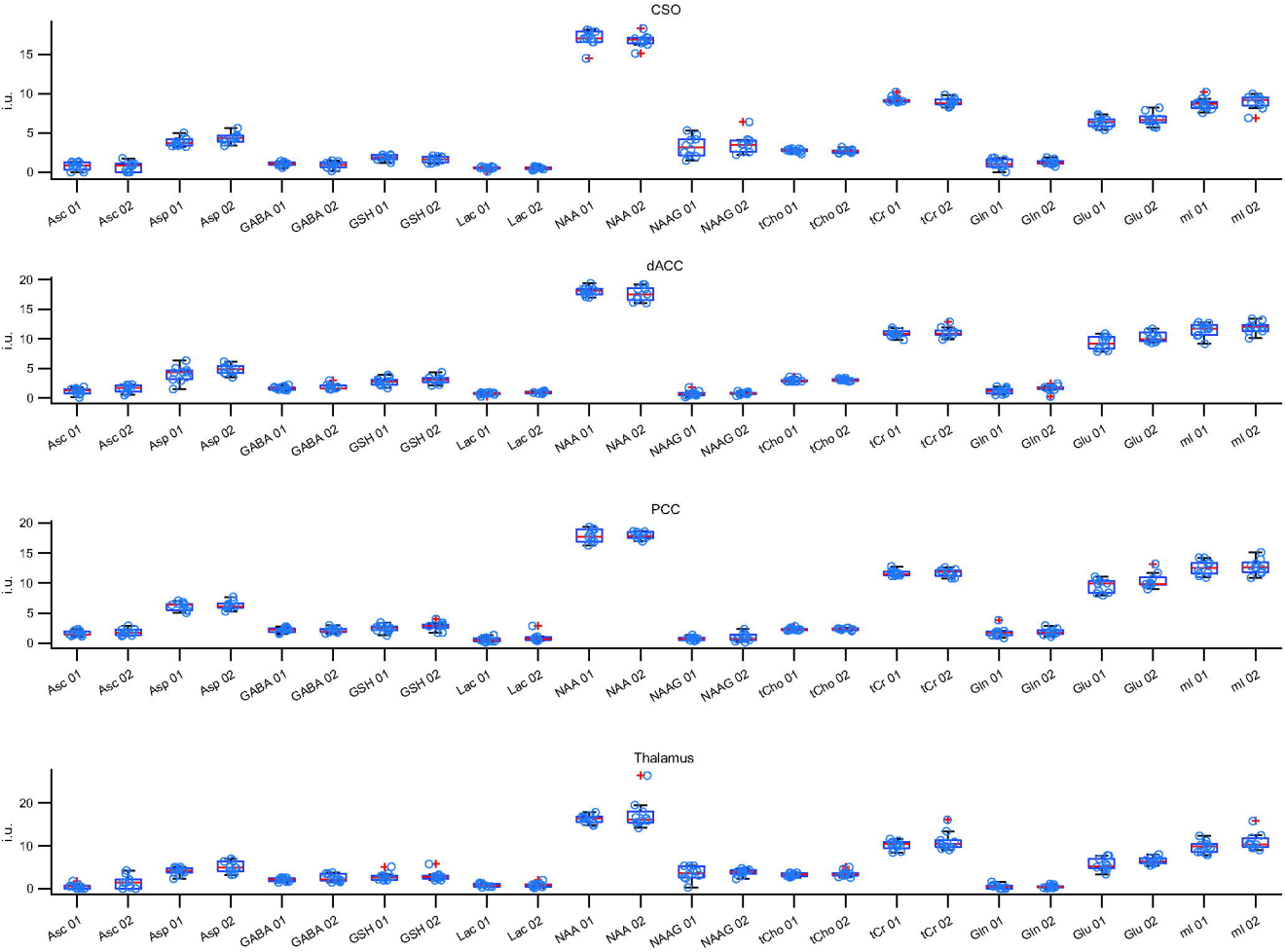
CSO
dACC
PCC
Thalamus
i.u.
Asc 01
Asc 02
Asp 01
Asp 02
GABA 01
GABA 02
GSH 01
GSH 02
Lac 01
Lac 02
NAA 01
NAA 02
NAAG 01
NAAG 02
tCho 01
tCho 02
tCr 01
tCr 02
Gln 01
Gln 02
Glu 01
Glu 02
mI 01
mI 02

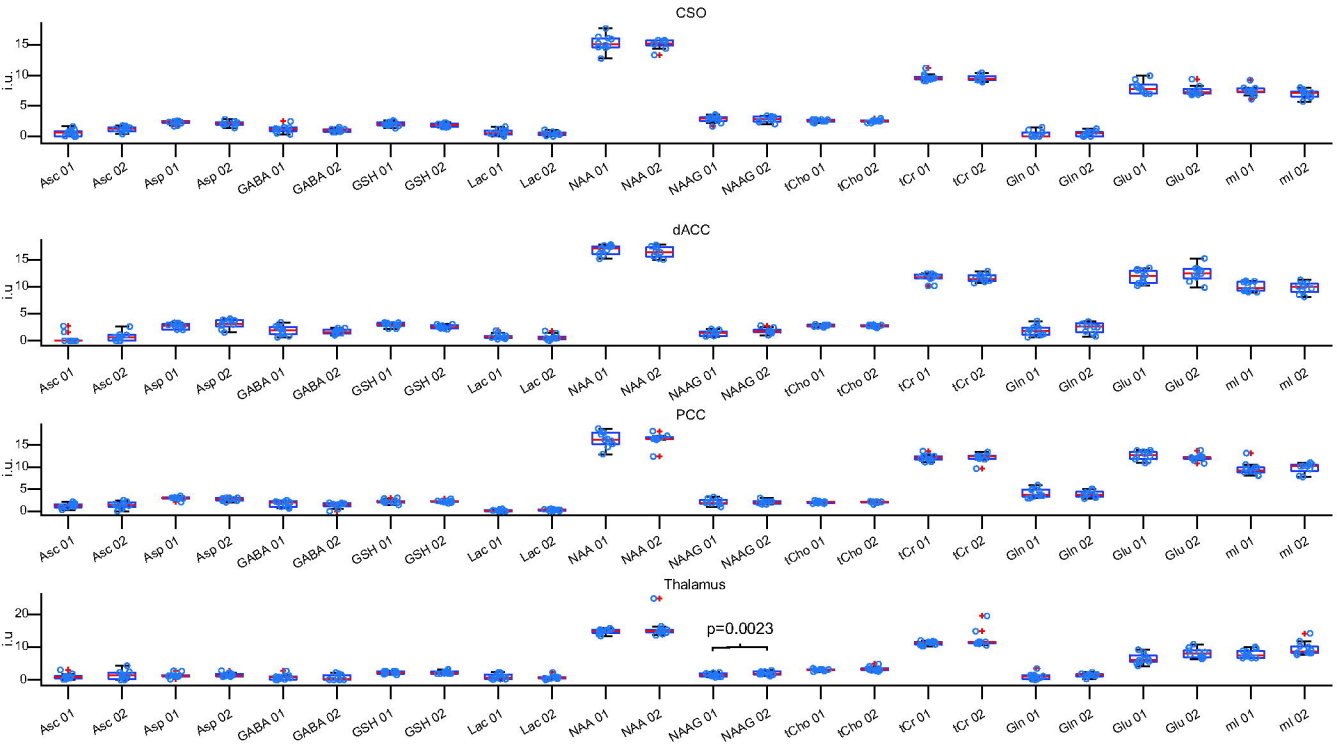
CSO
i.u.
dACC
i.u
PCC
i.u.
Thalamus
i.u
p=0.0023
Asc 01
Asc 02
Asp 01
Asp 02
GABA 01
GABA 02
GSH 01
GSH 02
Lac 01
Lac 02
NAA 01
NAA 02
NAAG 01
NAAG 02
tCho 01
tCho 02
tCr 01
tCr 02
Gln 01
Gln 02
Glu 01
Glu 02
mI 01
mI 02